*Journal of Thermal Analysis and Calorimetry, Vol. 89 (2007) 3, 847–852*

# SYNTHESIS AND CHARACTERIZATION OF ANTIBACTERIAL COMPOUNDS USING MONTMORILLONITE AND CHLORHEXIDINE ACETATE

*D. Yang*[1,2]*, P. Yuan*[1]*, J. X. Zhu*[1] *and H.-P. He*[1*,]

[1]Guangzhou Institute of Geochemistry, Chinese Academy of Sciences, Guangzhou 510640, China
[2]Graduate University of Chinese Academy of Sciences, Beijing 100039, China

Two series of antibacterial compounds were synthesized using montmorillonite and chlorhexidine acetate (CA) by ion-exchange reaction. The resulting samples were characterized by high-resolution thermogravimetric analysis (HRTG), Fourier transform infrared (FTIR) spectroscopy, X-ray diffraction (XRD) and their antibacterial activity was assayed by halo method. In this study, the loaded amounts of CA in the resultant compounds were evaluated by the HRTG curves. CA adopts a lateral monolayer arrangement in the resulting samples with low CA loading, while a special state with partial overlapping of organic molecules is supposed for the resulting samples prepared at 1.0–4.0 CEC. After the intercalation with CA, the hydrophilic surfaces of montmorillonite are changed to hydrophobic ones, reflected by the frequency shift of the symmetric $\nu_{1(O-H)}$ stretching vibration from low to high. This study shows that the interlayer cations in raw montmorillonite have little influence on the structure of the resulting samples. Antibacterial activity test against *E. coli* demonstrates that the antibacterial activity of the resulting samples strongly depends on the content of the loaded CA and these resulting materials show a long-term antibacterial activity that can last for at least one year.

***Keywords:*** *antibacterial materials, chlorhexidine acetate, high-resolution thermogravimetric analysis, interlayer structure, montmorillonite*

## Introduction

Synthesis and application of clay-based antibacterial materials have attracted great interest in recent years due to the worldwide concern about the public health [1]. The most commonly used clay in the preparation of antibacterial materials is montmorillonite [1–6]. Because of isomorphic substitution within the clay layers (for example, $Al^{3+}$ replaced by $Mg^{2+}$ or $Fe^{2+}$ in the octahedral sheet; $Si^{4+}$ replaced by $Al^{3+}$ in the tetrahedral sheet), the clay layer is negatively charged, which is counterbalanced by cations in the interlayer. These cations are exchangeable and can be replaced by antibacterial ions, resulting in a family of antibacterial materials. Meanwhile, clay minerals have an excellent adsorption property due to their high surface area. This makes clay minerals to be a good candidate to adsorb or fix virus, bacteria and other harmful substances onto their surface [5]. In addition, due to their low-cost and favourable thermal stability, clay minerals can be used as excellent carriers for synthesis of antibacterial materials.

According to the type of antibacterial components used, antibacterial materials can be divided into two basic types, i.e., inorganic and organic antibacterial materials. For synthesis of clay-based inorganic antibacterial materials, most antibacterial inorganic cations used are heavy metal such as $Ag^{+}$ [7–9] and $Cu^{2+}$ [2, 10–13]. However, the following problems and/or disadvantages arise in the synthesis and application of inorganic antibacterial materials with heavy metals: 1) An accumulation of heavy metals will result in serious environmental problem and may be harmful to human in the case of high metal concentration; 2) $Ag^{+}$ is not stable in aqueous solution and tends to be reduced to $Ag^{0}$ when exposed to light or heat. Meanwhile, $Ag^{+}$ is apt to precipitate with $Cl^{-}$, $HS^{-}$, $SO_4^{2-}$ and other commonly existing anions in natural water, losing the antibacterial activity. On the other hand, the cost for preparing antibacterial materials using silver is high [2].

Despite the relatively low stability (e.g. low decomposition temperature, low melting point, toxicity) [14], organic antibacterial materials show some advantages in the synthesis and application. For example, organic antibacterial materials display organophilicity, i.e., the compatibility with organic matrix such as textile, paints, polymer, etc. Meanwhile, bacteria are hydrophobic also, so organic antibacterial materials are easier to adhere to bacteria and then to sterilize it. What more important, recently, the study of organoclay-based nanocomposites has made

* Author for correspondence:hehp@gig.ac.cn

*1388–6150/$20.00*

*Akadémiai Kiadó, Budapest, Hungary*
*Springer, Dordrecht, The Netherlands*

great progress, in which organoclays were synthesized by modifying clay minerals with surfactants [15]. Organoclay-based nanocomposites often exhibit remarkable improvement in materials properties when compared with virgin polymer or conventional micro- and macro-composites [15]. These improvements can include high moduli, increased strength and heat resistance, decreased gas permeability and flammability, and increased biodegradability of biodegradable polymer [15]. In addition, Herrera *et al*. [5] revealed modified organoclay products could be useful in the treatment and clarifications of bacteria from various water sources. Here, a very interesting idea comes up with us that a new family of nanocomposites with antibacterial property can be synthesized using clays modified by some special organic reagent with antibacterial activity.

In this study, a kind of organoclay antibacterial compound was synthesized using montmorillonite and chlorhexidine acetate ($C_{22}H_{30}N_{10}Cl_2{\cdot}2C_2H_4O_2$). Chlorhexidine acetate (abbreviated as CA hereafter) is a bisbiguanide antiseptic and disinfectant which is bactericidal or bacteriostatic against a wide range of Gram-positive and Gram-negative bacteria [16]. CA has been widely used for diminishing inflammation, disinfecting, washing surface of a wound [17]. The structure of the resulting samples was characterized by X-ray diffraction (XRD), Fourier transform infrared (FTIR) spectroscopy and high-resolution thermogravimetric measurement (HRTG). Their antibacterial activity was assayed by so-called halo method. This is a preliminary step for the preparation of polymer/clay nanocomposites with antibacterial activity.

## Experimental

### *Materials*

Montmorillonite (CaMt) from Hebei, China, was purified and classified by the sedimentation method. The <2 μm fraction was collected and dried at 100°C. Then, the sample was ground through a 200-mesh sieve and sealed in a glass bottle for further use. The cation exchange capacity (CEC) of CaMt is 0.80 eq $kg^{-1}$, determined by $NH_4^+$ exchanging method as described in the literature [18]. The structural formula of CaMt calculated from the result of chemical analysis (not known) and cation exchange capacity measurements can be expressed as $(Na_{0.05}Ca_{0.18}Mg_{0.10})[Al_{1.58}Fe_{0.03}Mg_{0.39}][(Si_{3.77}Al_{0.23})]O_{10}(OH)_2{\cdot}nH_2O$. Its Na-saturated used in this study form (NaMt) was prepared by ion exchange reaction between CaMt and $Na_2CO_3$, as previously described [19].

Chlorhexidine acetate ($C_{22}H_{30}N_{10}Cl_2{\cdot}2C_2H_4O_2$) was provided by Jiutai Pharmaceutical Co. Ltd., Jinzhou, China. Ethanol was analytical grade without further purification.

### *Synthesis of antibacterial compounds*

The synthesis of montmorillonite–chlorhexidine acetate compounds was performed by the following procedure. 2 g of montmorillonite (CaMt or NaMt) was dispersed in about 30 mL of distilled water and a desired amount of CA was dissolved in 70 mL of ethanol. The concentrations of CA used are 0.2, 1.0, 2.0, 3.0 and 4.0 CEC of montmorillonite, respectively. Then, the two solutions were mixed together and magnetic stirred for 2 days at room temperature. All products were washed twelve times with ethanol about 30 mL for each washing, dried at 100°C and ground in an agate mortar to pass through a 200-mesh sieve. The sample prepared at the CA concentration of 1.0 CEC, using CaMt as a carrier, was marked as CaMt-1.0 and the others were marked in a similar way.

### *Characterization*

XRD was performed on unoriented samples using a Rigaku D/max-1200 diffractometer with $CuK_\alpha$ radiation under target voltage 40 kV and current 30 mA. All samples were recorded between 3 and 20° (2θ) at a scanning speed of 8° (2θ) $min^{-1}$.

HRTG analysis was performed on a TA Instruments Inc., Q500 thermobalance. Samples were heated from room temperature to 1000°C at a heating rate of 10°C $min^{-1}$ with a resolution of 6°C under $N^2$ atmosphere (80 $cm^3$ $min^{-1}$). Approximately 30 mg of finely ground sample was heated in an open platinum crucible.

FTIR spectra were conducted on Perkin-Elmer 1725X Fourier transform infrared spectrometer by the KBr pressed disk technique. For each sample, 0.7 mg of sample and 70 mg of dry KBr were weighed and then were ground in an agate mortar for 10 min before making the pellets. Analyses were performed in the transmission between 300 and 4000 $cm^{-1}$, with a resolution of 2 $cm^{-1}$ and accumulation of 64 scans.

### *Antibacterial activity assay*

Antibacterial activity was assayed by so-called halo method [3] as follows. A beef agar medium melted was poured in a Petri dish and solidified. Then, the medium containing bacteria ($1{\cdot}10^6$ cells of *E. coli* per ml) was layered over it. The sample about 0.5 g was put on it and then incubated it. Incubation conditions were 1 day at 37°C. Antibacterial activity was evaluated by the transparent halo circle around the specimen after incubation. That is to say, when a specimen has antibacterial activity, the halo circle is

formed along the periphery of the specimen, and the width of the halo increases with the increase of antibacterial activity of the specimen. All glassware used in this study was sterilized in the autoclave at 120°C for 30 min before each experiment to exclude any possible microbial disturbance.

## Results and discussion

*XRD and HRTG analysis*

The XRD patterns of montmorillonite and the resulting samples were shown in Fig. 1. The basal reflection ($d_{001}$) of NaMt is 1.22 nm. For the series of the synthesized samples using NaMt as the carrier, the $d_{001}$ value of NaMt-0.2 is (1.45 nm) larger than that of NaMt (1.22 nm). This indicates that CA has been intercalated into the montmorillonite interlayer. As well known, the layer thickness of montmorillonite is ca. 0.96 nm; hence, the interlayer height of NaMt-0.2 should be ca. 0.49 nm. This value almost equals to the height of CA molecules (0.5 nm) when they lie flat, corresponding to a lateral monolayer arrangement for CA in the montmorillonite interlayer.

When using CaMt as a carrier, the basal spacing of CaMt-0.2 is ca. 1.50 nm (Fig. 1), similar to that of raw CaMt. On the basis of its basal spacing, it is difficult to determine whether CA has been intercalated into the montmorillonite interlayer. To ascertain whether CA has been intercalated into montmorillonite interlayer, thermal analyses of CaMt and CaMt-0.2 were conducted (shown in Fig. 2). The DTG curve of CaMt displays four peaks at 42, 115, 633 and 915°C, respectively. The peaks at 42, 115 and 633°C correspond to the losses of adsorbed water, hydrated water of the interlayer cations and the structural hydroxyls, respectively. The peak at ca. 915°C should be attributed to phase transformation from montmorillonite to spinel, cristobalite, mullite, and/or pyroxenes (enstatite) [20]. However, besides the above-mentioned peaks corresponding to montmorillonite, three prominent peaks at 218, 294 and 375°C, respectively, were recorded in the DTG curve of CaMt-0.2. Since montmorillonite is thermally stable in the temperature range of 200–500°C, these three peaks should result from CA. The peak at 218°C corresponds to the evaporation of physically adsorbed CA while the peaks at 294 and 375°C to the decomposition of the intercalated CA within the clay interlayer. Hence, the mass loss of CaMt-0.2 in this temperature range should be attributed to the evaporation and/or decomposition of CA intercalated into montmorillonite interlayer [21, 22]. This demonstrates that CA has been intercalated into montmorillonite interlayer.

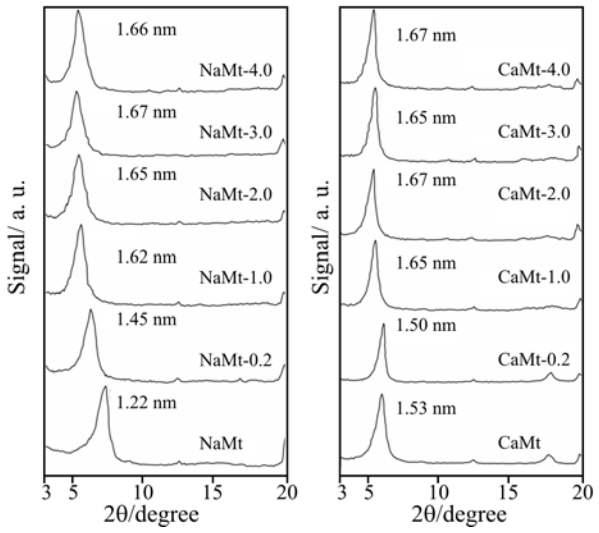


**Fig. 1** X-ray diffraction patterns of CaMt, NaMt and the resulting compounds

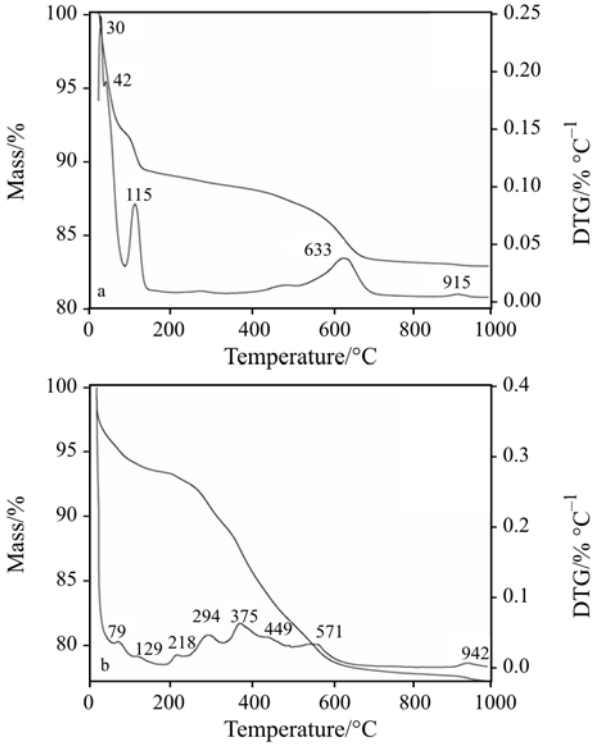


**Fig. 2** HRTG and DTG curves of a – CaMt and b – CaMt-0.2

When the CA concentration increased to 1.0–4.0 CEC, the basal reflections of the synthesized antibacterial compounds from both CaMt and NaMt locate at 1.62–1.67 nm (Fig. 1). There is no prominent difference among the $d_{001}$ values of these compounds. An evaluated interlayer height is 0.66–0.71 nm, deduced from the *d* values and the TOT layer thickness. This interlayer distance is bigger than that when CA molecules adopt lateral monolayer (0.5 nm), but

smaller than that of lateral bilayer (ca. 1.0 nm). Table 1 shows the results of HRTG analyses of the resulting samples, which demonstrates that the CA loadings in these samples prepared using NaMt and CaMt are 15.56–16.26 and 18.82–19.10%, respectively. Based on the results of XRD, both sodium and calcium montmorillonite reach the maximum of $d_{001}$ values for 1.0–2.0 CEC compounds. After this range (1.0–2.0 CEC), the CA concentration during the preparation has little effect on $d_{001}$ values of the resulting samples, reflecting that a saturation state was achieved. XRD and HRTG data suggest that in CaMt the saturation was reached at 1.0 CEC, whereas for NaMt at 2.0 EC. In the study of organic-modified clays, Favre and Lagaly (1991) [23] proposed that this $d_{001}$ value corresponds to a 'kink' structure. Recently, our molecular modeling of organic clays demonstrates a transition structure from lateral-monolayer to lateral-bilayer, in which a partial overlapping of organic molecules was observed [24]. However, in our present study, even the CA concentration increased to 4.0 CEC, the basal spacing of the resultant antibacterial compound is still remained at ca. 1.66 nm. Both of the almost unchanged interlayer height and CA loading reflect that the interlayer structure of the synthesized compounds at 1.0–4.0 CEC is similar. This might be resulted from the complex structure of CA molecules with a phenyl at the two opposite ends, respectively. The arrangement model for CA in the montmorillonite interlayer is very different from those of quaternary alkylammonium modified montmorillonites [19, 23], in which various surfactant arrangement models (e.g. lateral monolayer, lateral bilayer, pseudotrilater, paraffin monolayer, paraffin bilayer) were observed, depending on the loading of the intercalated surfactant.

For the antibacterial compounds prepared at the CA concentrations of 1.0–4.0 CEC, their basal spacings are similar to those prepared from NaMt, reflecting similar interlayer structure within them. This study shows that the interlayer cations (e.g. $Ca^{2+}$, $Na^{+}$) in raw montmorillonites have little influence on the structure of the resulting samples whereas the CA loading in the antibacterial compounds prepared from CaMt (ca. 19%) is higher than that prepared from NaMt (ca. 16%) at the same CA concentrations (Table 1). The variation of CA loadings in the resulting samples has a significant influence on their antibacterial activity as demonstrated by antibacterial tests (see antibacterial test).

*FTIR spectra*

FTIR spectra is an useful technology to investigate the microstructure and surface property of clays and related materials [25–28]. The IR spectra of CA and CaMt, CaMt-0.2 are showed in Fig. 3. The wavenumber and assignment of the vibration modes observed are listed in Table 2. The assignments are based on previous reports on montmotillonite [27, 29]. It is found that FTIR spectra of all samples display a band at ca. 3620 $cm^{-1}$, corresponding to the O–H stretching vibration of the structural hydroxyl groups. The IR spectra of the two series of resulting samples are similar to that CaMt-0.2. However, there is difference between those of raw montmorillonite and resulting samples. After the intercalation of CA, the adsorption band at ca. 3420 $cm^{-1}$ corresponding to the symmetric $\nu_{1(O-H)}$ stretching vibration band of adsorbed water shifts to higher frequency at ca. 3483 $cm^{-1}$, reflecting a decrease of adsorbed water in external surface or in the interlayer spaces of montmorillonite [26, 30]. This suggests that the hydrophilicity of montmorillonite surface decreases and the hydrophobicity increases after the intercalation of CA. In addition, the ab-

**Table 1** The CA loadings (mass%) in the resulting compounds synthesized at different CA concentrations

| Sample | CA loadings/ mass% | Sample | CA loadings/ mass% |
|---|---|---|---|
| CaMt-0.2 | 10.73 | NaMt-0.2 | 6.71 |
| CaMt-1.0 | 19.10 | NaMt-1.0 | 15.56 |
| CaMt-2.0 | 18.86 | NaMt-2.0 | 16.26 |
| CaMt-3.0 | 18.82 | NaMt-3.0 | 15.85 |
| CaMt-4.0 | 18.95 | NaMt-4.0 | 16.03 |

The CA loadings are deduced from the corresponding HRTG curves as follows: the total mass loss is obtained by the TG curve, and then the mass loss associated with dehydroxylation of montmorillonite is calculated according to the mass of the residual at ca. 1000°C. The quantity of the total mass loss subtracting the mass loss associated with dehydroxylation of montmorillonite is the CA loadings.

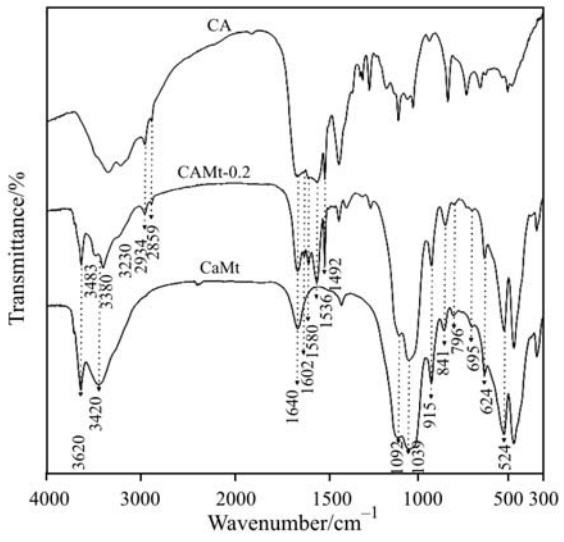


**Fig. 3** FTIR spectra of CaMt, CaMt-0.2 and CA

**Table 2** Positions and assignments of the observed FTIR vibration bands

| Position/cm$^{-1}$ | Assignments |
|---|---|
| 3620 | OH stretching of structural hydroxyl groups |
| 3483 | OH stretching of water |
| 3420 | OH stretching of water |
| 3380 | N–H stretching |
| 3230 | Ar–H stretching |
| 2934 | $CH_2$ C–H antisymmetric stretching |
| 2859 | $CH_2$ C–H symmetric stretching |
| 1640 | OH deformation of water and C–N stretching |
| 1602, 1580, 1536, 1492 | aromatic C=C stretching |
| 1414, 1371 | inter ring C–C stretching |
| 1290, 1245 | C–N stretching |
| 1092 | Si–O stretching (longitudinal mode) |
| 1039 | Si–O–Si stretching |
| 915 | AlAlOH deformation |
| 841 | AlMgOH deformation |
| 796 | Si–O stretching of quartz and silica |
| 695 | Si–O stretching |
| 624 | coupled Al–O and Si–O, out of plane |
| 524 | Al–O–Si deformation |

sorptions at ca. 3380 and 3230 cm$^{-1}$ are attributed to the N–H and C–H stretching vibrations of the aromatic ring of CA and those at ca. 2859 and 2934 cm$^{-1}$ to the symmetric and asymmetric stretching vibrations of the methylene groups of CA [31]. The absorption bands in the region of 1200–1600 cm$^{-1}$ also resulted from C–N and C–C vibrations of CA. Here, it can be found that FTIR spectra of montmorillonite and the resulting compounds provide complementary informations that CA has been intercalated into montmorillonite interlayer spaces and the hydrophilic surface of montmorillonite was changed to hydrophobic one after the intercalation of CA. This transformation can enhance affinity of the organic antibacterial compounds to bacteria.

*Antibacterial test*

The halo test results of CaMt, NaMt and the resulting samples are shown in Figs 4 and 5, respectively. Both of raw montmorillonites (CaMt and NaMt) and the resulting samples prepared at 0.2 CEC (CaMt-0.2 and NaMt-0.2) show no halo circle for *E. coli*, reflecting no antibacterial activity for these samples. However, all the resulting samples synthesized at the CA concentration of 1.0–4.0 CEC from both CaMt and NaMt, have a prominent halo circle around the specimen. This reflects that the antibacterial activity of the corresponding samples strongly depends on the CA loading. Meanwhile, a comparison between the halo test results of the two series of compounds (resulted from CaMt and NaMt, respectively) indicates that the synthesized samples from CaMt display a better antibacterial property than those from NaMt do. This should be attributed to the higher CA loading in the antibacterial compounds from CaMt than from NaMt as indicated by HRTG analysis results (Table 1), namely, the antibacterial activity of the resulting samples increases with an increase of the CA loading.

The halo test results of CaMt-2.0 and NaMt-2.0 one year later are shown in Figs 4(7) and 5(7). The clearly recorded halo circle demonstrates that the antibacterial activity of the synthesized compounds can last for a long period. It is of high importance for the application of synthesized antibacterial materials.

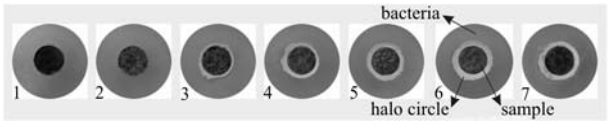


**Fig. 4** Halo test results of CaMt and the resulting compounds; 1 – CaMt; 2 – CaMt-0.2; 3 – CaMt-1.0; 4 – CaMt-2.0; 5 – CaMt-3.0; 6 – CaMt-4.0; 7 – CaMt-2.0 (test conducted after one year)


**Fig. 5** Halo test results of NaMt and the resulting compounds; 1 – NaMt; 2 – NaMt-0.2; 3 – NaMt-1.0; 4 – NaMt-2.0; 5 – NaMt-3.0; 6 – NaMt-4.0; 7 – NaMt-2.0 (test conducted after one year)

## Conclusions

In this study, organic antibacterial compounds were synthesized using montmorillonite and Chlorhexidine acetate. XRD patterns demonstrate that CA ions have been intercalated into clay interlayer. The arrangement of CA ions within the interlayer of antibacterial compound prepared at 0.2 CEC belongs to a lateral monolayer. And CA ions are supposed to be a special state with partial overlapping of organic molecules for the compounds prepared at 1.0–4.0 CEC. This interlayer structure is very different from quaternary alkylammonium modified montmorillonites, resulted from its complex molecular conformation. This study shows that the interlayer cations (e.g. $Ca^{2+}$, $Na^{+}$) in

raw montmorillonite have little influence on the structure of the resultant antibacterial compounds.

Antibacterial activity test against *E. coli* demonstrates that the raw montmorillonite and the compounds prepared at low CA concentration (0.2 CEC) do not show antibacterial activity. The antibacterial activity of the resultant compounds strongly depends on the CA loading, i.e., the antibacterial activity of the antibacterial compounds increases with the increase of CA loading. After one year, the halo test demonstrates that the antibacterial compounds still show excellent antibacterial activity, indicating that the antibacterial activity of the compounds can last for a long period.

## Acknowledgements

This work was funded by Natural Science Foundation of Guangdong Province (Grant No. 023203) and Scientific and Technological Project of Guangdong Province, China (Grant No. 013109). The authors are grateful to Dr. Q. Tao for his assistance to this work.

## References

1 Y. L. Ma, Z. R. Xu, T. Guo and P. You, J. Colloid Interf. Sci., 280 (2004) 283.
2 Y. H. Zhou, M. S. Xia, Y. Ye and C. H. Hu, Appl. Clay Sci., 27 (2004) 215.
3 A. Oya, T. Banse, F. Ohashi and S. Otani, Appl. Clay Sci., 6 (1991) 135.
4 F. Ohashi, A. Oya, L. Duclaux and F. Beguin, Appl. Clay Sci., 12 (1998) 435.
5 P. Herrera, R. C. Burghardt and T. D. Phillips, Vet. Microbiol., 74 (2000) 259.
6 Z. Yamada, K. Ohta and S. Takauchi, Kagaku Kogaku Ronbun., 17 (1991) 29.
7 Y. Onodera, T. Iwasaki, A. Chatterjee, T. Ebina, T. Satoh, T. Suzuki and H. Mimura, Appl. Clay Sci., 18 (2001) 123.
8 F. Ohashi and A. Oya, Agents, 20 (1992) 525.
9 F. Ohashi and A. Oya, Appl. Clay Sci., 6 (1992) 301.
10 Y. Ye, Y. H. Zhou, M. S. Xia, C. H. Hu and H. F. Ling, J. Inorg. Mater., 18 (2003) 569.
11 C. H. Hu, Z. R. Xu and M. S. Xia, Vet. Microbiol., 109 (2005) 83.
12 C. H. Hu and M. S. Xia, Appl. Clay Sci., 31 (2006) 180.
13 T. Guo, Y. L. Ma, P. Guo and Z. R. Xu, Vet. Microbiol., 105 (2005) 113.
14 B. W. Li, S. H. Yu, J. Y. Hwang and S. Z. Shi, J. Miner. Mater. Character. Eng., 1 (2002) 61.
15 S. S. Ray and M. Okamoto, Prog. Polym. Sci., 28 (2003) 1539.
16 Martindale, The Complete Drug Reference, Pharmaeceutical Press, London 1999.
17 S. Shani, M. Friedman and D. Steinberg, Caries Res., 34 (2000) 260.
18 H. P. He, J. G. Guo, X. D. Xie and J. L. Peng, Environ. Int., 26 (2001) 347.
19 J. X. Zhu, H. P. He, J. G. Guo, D. Yang and X. D. Xie, Chin. Sci. Bull., 48 (2003) 368.
20 R. E. Grim, Clay Mineralogy, McGraw-Hill, New York 1968.
21 Y. Xi, W. Martens, H. He and R. L. Frost, J. Therm. Anal. Cal., 81 (2005) 91.
22 S. Yariv, Appl. Clay Sci., 24 (2004) 225.
23 H. Favre and G. Lagaly, Clay Miner., 26 (1991) 19.
24 H. P. He, J. Galy and J. F. Gerard, J. Phys. Chem. B, 109 (2005) 13301.
25 H. P. He, R. L. Frost and J. X. Zhu, Spectrochim. Acta A, 60 (2004) 2853.
26 C. T. Johnston, G. Sposito and C. Erickson, Clays Clay Miner., 40 (1992) 722.
27 J. Madejova and P. Komadel, Clays Clay Miner., 49 (2001) 410.
28 M. L. McKelvy, T. R. Britt, B. L. Davis, J. K. Gillie, L. A. Lentz, A. Leugers, R. A. Nyquist and C. L. Putzig, Anal. Chem., 68 (1996) 93R.
29 G. M. Do Nascimento, V. R. L. Constantino and M. L. A. Temperini, J. Phys. Chem. B, 108 (2004) 5564.
30 W. Z. Xu, C. T. Johnston, P. Parker and S. F. Agnew, Clay Clay Miner., 48 (2000) 120.
31 Y. Q. Li and H. Ishida, Langmuir, 19 (2003) 2479.

Received: December 28, 2006
Accepted: March 17, 2007

DOI: 10.1007/s10973-006-8318-3